ELSEVIER

Bone 39 (2006) 1196 – 1202

BONE

www.elsevier.com/locate/bone

The interaction of microstructure and volume fraction in predicting failure in cancellous bone

Ara Nazarian [a,b], Martin Stauber [b], David Zurakowski [c], Brian D. Snyder [a,c], Ralph Müller [b,*]

[a] *Orthopedic Biomechanics Laboratory, Beth Israel Deaconess Medical Center and Harvard Medical School, Boston, MA, USA*
[b] *Institute for Biomedical Engineering, University and ETH Zürich, Moussonstrasse 18, 8044 Zürich, Switzerland*
[c] *Department of Orthopaedic Surgery, Children's Hospital and Harvard Medical School Boston, MA, USA*

Received 11 October 2005; revised 23 March 2006; accepted 27 June 2006
Available online 21 August 2006

Abstract

Inroads have been made in the diagnosis and treatment of osteoporosis, yet dual-energy X-ray absorptiometry is still the primary diagnostic modality. This method provides 2D projections of an irregular 3D construct. However, human cancellous bone is highly heterogeneous with varying material properties. Therefore, to properly assess fracture risk, it is imperative to take into consideration microstructural indices besides subregional bone volume fraction (BV/TV).

A power law model with average BV/TV as the independent variable describes 38% of the variation in yield strength; however, this predictive power is increased to 56% when BV/TV of the weakest subregion is considered. Of twenty-five specimens studied, 76% had minimum BV/TV, maximum principal Eigen value of the fabric tensor (H_1) and minimum connectivity density (Conn.D) values within the visually determined failure regions. These three independent morphometric indices yielded significant differences between the failure and non-failure regions of each specimen.

From the results, we conclude that subregions with minimal BV/TV values are better predictors of mechanical failure in cancellous bone than average specimen BV/TV. Addition of microstructural indices augments this predictive power to generate a trabecular failure prediction model based on volume fraction and cancellous bone microstructure specifically in areas where trabecular failure is most likely to occur.

Keywords: Cancellous bone; Failure prediction; BV/TV; Morphometric indices; Probability

Introduction

Osteoporosis is defined as a skeletal disorder characterized by compromised bone strength predisposing to an increased risk of fracture. Bone strength reflects the integration of two main features: bone density and bone quality, where bone quality refers to architecture, turnover, damage accumulation (e.g., microfractures) and mineralization [2]. This disease, currently considered an epidemic in most developed countries, is affecting approximately one in three Caucasian women over the age of 65 and is expressed by greatly reducing bone strength while concurrently increasing fracture risk. The increased social and health care costs associated with the complications of this disease have promoted extensive research in establishing preventative and screening methodologies and guidelines for those affected or most likely to be affected.

One of the most cost-effective and widespread methods to assess fracture risk in osteoporotic patients has been the advent and application of dual-energy X-ray absorptiometry (DXA) [1]. This technique facilitates the measurement of bone mass (BMC) and areal bone mineral density (BMD) as well as certain measures of compressive and bending strength of bone [3]. These measures are extremely accurate for homogeneous materials undergoing a known loading mode. Nevertheless, human cancellous bone consists of a non-uniform network of trabecular elements undergoing complex loading patterns, where structure seems to play an important role on top of the material per se [19].

It has been established that mechanical properties of cancellous bone are primarily dependent upon its apparent density [4,27]. However, the variation of cancellous bone

* Corresponding author. Fax: +41 44 632 1214.
E-mail address: ralph.mueller@ethz.ch (R. Müller).

8756-3282/$ - see front matter © 2006 Elsevier Inc. All rights reserved.
doi:10.1016/j.bone.2006.06.013

microstructure at a given volume fraction level has resulted in a stiffness and strength variation much higher than those observed in most other types of cellular solids [6]. The complex interaction of volume fraction and microstructure compounded by other issues such as increasing deviation from continuum mechanics principles (e.g., highly osteoporotic samples), loading direction, anatomic site, intraspecimen variations and artifacts associated with mechanical testing protocols have hindered efforts to reach a consensus on the nature of the relationship between bone mechanical properties and its failure behavior. This is especially important for specimens from osteoporotic patients, where bone volume fraction range is considerably lower than those observed in normal bone. Moreover, trabecular network is not evenly distributed across any cancellous bone site as cancellous bone volume fraction variation is rather large within any anatomic region [10]. It has also been demonstrated that bone failure may not be evenly distributed over the whole specimen, but occurs in well defined bands [22,23,29], leaving the remaining portion of the microstructure intact. The importance of band-like failure is essential in the correct assessment of modulus of elasticity which is hampered by the fact that strains are not uniform along the sample length, therefore violating an important requirement in continuum mechanics.

The contribution of microstructure to the mechanical properties of cancellous bone has been widely accepted [17,26], and to this end, many indices have been devised to further describe the influence of changes in bone microstructure onto its mechanical properties [7–9,20,24,25]. However, these methods present an average number for the entire specimen and do not take into consideration general inhomogeneities and local variations in bone microstructure. Therefore, it is imperative that the weakest link in cancellous bone is identified, and its contribution to the failure properties of whole bone evaluated.

To this end, we aim to show that bone volume fraction of the weakest subregions, in a trabecular bone specimen *of the same size and located at the same site*, is a better predictor of its failure than bone volume fraction averaged over the entire sample and that microstructural indices from the subregions of trabecular failure can be incorporated in statistical models to predict mechanical failure of trabecular bone specimens accurately.

Materials and methods

Materials

A group of 25 human vertebral cancellous bone specimens were cored from thoracic and lumbar regions of vertebral bodies harvested from 2 spines of donors from Anatomic Gift Program at Harvard University (65 y/o M, 63 y/o F). The bone specimens were cored parallel to the anatomical axis out of a pre-cut block of the vertebral body using a diamond coring tool (Starlite Industries, Rosemont, PA) while completely submerged in 0.9% saline solution. All specimens were stored in saline-soaked gauze at a temperature of −20°C. Once cored, the two ends of all specimens were cut perpendicular to the anatomical axis between two parallel diamond wafering blades running on a low-speed saw (Isomet, Buehler Corp., Lake Bluff, IL) following previously described protocols [22,23]. The specimens were cored and cut using a 3:2 ratio (H 11.62±0.14 mm and ∅ 7.85±0.21 mm) between length and diameter. Before testing, pre-aligned brass end caps with a 9 mm diameter and 1.2 mm in thickness were glued with cyanoacrylate (American Glue Corp., Taylor, MI) to both ends of the specimens. This step effectively reduced end artifact [15] by restraining displacement at either end of the specimen and providing support to the free ends of the trabeculae. The specimens remained wet during testing with the humidity sealed within the micro-compression device. This was verified upon retrieval of wet specimens at the end of testing periods.

Mechanical testing and data reconstruction of trabecular bone specimens

A previously described and validated mechanical testing and data acquisition (MTDAQ) device was employed for this study [22,23]. This method incorporates stepwise micro-compression in combination with time-lapsed micro-computed tomographic imaging (μCT) to study the 3D failure behavior of cellular solids, a method previously referred to as image guided failure assessment (IGFA) [18]. All specimens were preconditioned to eliminate typical toe behavior [13–15,18] at a strain rate of 0.005 s^{-1} for 7 cycles. The specimens were then transferred to the μCT scanner for initial imaging of the specimen in the intact state (0%). After imaging, the specimen was returned to the MTDAQ, and exposed to a monocyclic nominal strain of 2% at a strain rate of 0.01 s^{-1}. Following the application of each strain step, the specimen was allowed to relax for 20 min prior to the next μCT imaging. The twenty-minute time interval was necessary to allow for adequate stress relaxation in the specimen due to its viscoelastic material properties. This procedure was repeated five more times to acquire additional time-lapsed images at 4%, 8%, 12%, 16% and 20% nominal strain in the post-failure regime. Each imaging step was approximately 75 min in duration. The discrete stepwise mechanical data for each specimen were reconstructed as described previously [23].

Mechanical data analysis

The mechanical data were re-sampled and averaged to obtain stresses between 0% and 2% strain at intervals of 0.2% strain and between 2% and 20% strain at intervals of 1% strain. Modulus of elasticity, stiffness, yield strain and strength, ultimate strain and strength and ultimate load were calculated accordingly. The modulus of elasticity and the stiffness were determined by fitting a straight line parallel to the linear regions of the stress–strain and load–displacement curves respectively. Ultimate load and stress were defined as the initial peak load/stress and their corresponding displacement/strain as ultimate displacement and strain.

μCT imaging methods and image and data analysis

Progressive images were generated using a micro-tomographic imaging system (μCT 20, Scanco Medical AG, Bassersdorf, Switzerland) [28]. Measurements were stored in three-dimensional image arrays with isotropic voxel sizes of 34 μm. A three-dimensional Gaussian filter (σ=1.2) with a limited, finite filter support [2] was used to suppress the noise in the volumes. These images were binarized to separate bone from background using a global thresholding procedure [21] at 22.4%. To these images, a component labeling algorithm was applied to keep only the largest connected bone component and to remove small particles arising from noise and artifacts.

Each specimen's μCT image was divided along the longitudinal axis into 10 subregions of equal height. For each of these subregions, as well as for the whole specimen, direct 3D indices were computed [10]: bone volume fraction (BV/TV), bone surface density (BS/TV), specific bone surface (BS/BV), structure model index (SMI), trabecular number (Tb.N), trabecular thickness (Tb.Th), fabric tensor Eigen values (H_1–H_3), degree of anisotropy (DA=H_1/H_3) and connectivity density (Conn.D). In order to avoid boundary artifacts for the calculations of microstructural indices in the analyzed subregions, we performed morphometric evaluation of the entire specimen and then averaged out the data over each subregion using an appropriate masking procedure as provided by the CT manufacturer software (IPL, Scanco Medical AG, Bassersdorf, Switzerland).

The 3D images of each compression step were combined into an animation since 3D animations of the mechanical experiments contribute significantly to

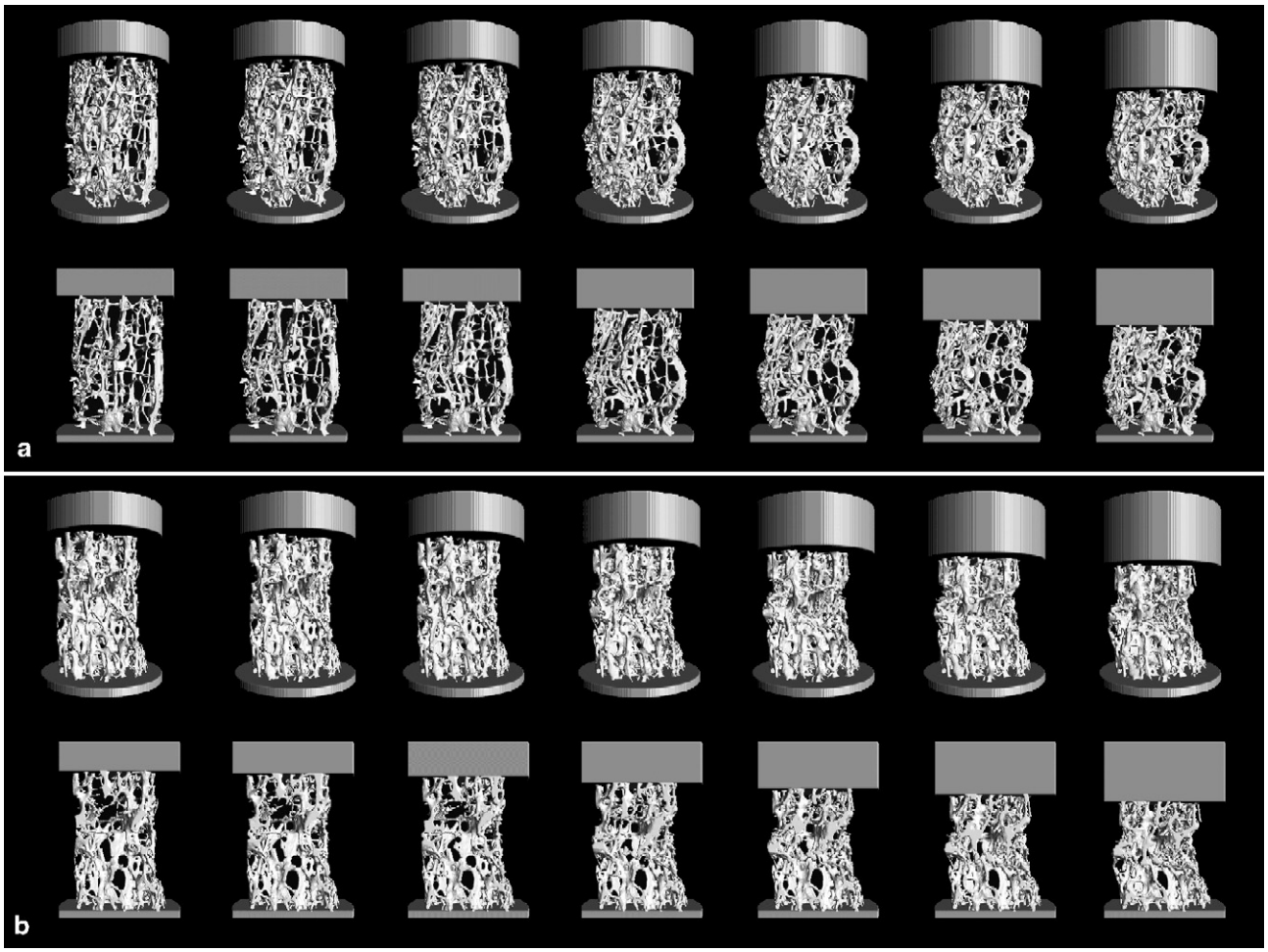

Fig. 1. Compression steps of 0, 2, 4, 8, 12, 16 and 20% global strain from two representative trabecular bone specimens (a and b). The top row, for each specimen, shows a front view of the entire specimen, and the second row demonstrates a representative coronal view of the same specimen viewed from the front.

the understanding of specimen failure. For this purpose, the 3D images had to be aligned initially with respect to the bottom end plate since this plate was fixed during the experiment. An algorithm was used to find the last plane of this end plate in each 3D image, enabling an alignment of the images along the perpendicular axis. A subsequent 2D correlation procedure was used in the first five bottom planes in order to perform alignment. Each aligned 3D dataset was then visualized under the same conditions (orientation, light settings) by using an extended Marching Cubes algorithm [16]. The resulting images were finally turned into an animation to visualize failure for all specimens (Figs. 1a–b). This procedure was done for four main directions (front, left, back, right) for the whole specimen as well as for two directions (front, left) for the 110 central slices (3.74 mm), which were used to visually identify the region(s) of failure (FX) and non-failure (NF). Each image was axially divided into 10 subregions of equal height, and failure was assigned to one or several of those subregions (Fig. 2). Two operators performed this process independently, and the individual results were pooled to obtain the final FX and NF regions. The same regions were used to determine local morphometric parameters. These morphometric indices were then related to the visually determined region(s) of failure.

The morphometric indices of the 10 subregions were normalized (against the subregion with the highest value for each index) and were ranked from 1 to 10, one being the least likely to fail and ten the most. Mean ranks of the FX and NF regions were then calculated for each specimen.

Statistical analysis

The Kolmogorov–Smirnov goodness-of-fit test was performed to check for normality of continuous morphometric indices in order to determine whether parametric or non-parametric methods were appropriate for analysis. Univariate analysis was performed to compare morphometric indices between failure and non-failure groups using two-sample Student's *t* test. In addition, multivariate stepwise logistic regression based on maximum

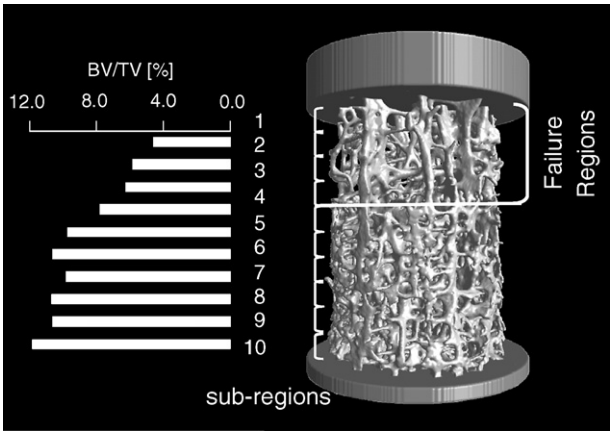

Fig. 2. Failure occurs at subregions with the lowest BV/TV values. Subregions number 1, 2, 3 and 4 with the lowest BV/TV values here coincide with the 4 regions that fail based on the visual data provided by the time-lapsed mechanical testing.

Table 1
Descriptive statistics for densitometric and mechanical analysis performed on all specimens

	Mass [g]	Apparent density [kg/m^3]	Yield strain [%]	Yield strength [MPa]	Ultimate strain [%]	Ultimate strength [MPa]	Modulus of elasticity [MPa]
Mean	0.22	0.38	1.60	0.95	2.01	1.02	59.69
SD	0.07	0.11	0.56	0.47	0.69	0.47	21.00
Minimum	0.10	0.18	0.63	0.32	0.86	0.36	27.58
Maximum	0.34	0.63	2.85	2.25	4.11	2.34	121.35
CV (%)	30.4	29.0	35.2	49.2	34.4	46.7	35.18

likelihood estimation (MLE) was used to identify significant predictors of failure using thirteen morphometric indices as candidate variables tested in the model. The likelihood ratio test was used to assess significance of the variables selected in the final model based on a backward selection procedure [11]. Model fit was evaluated by the Hosmer–Lemeshow statistic using a chi-square distribution [12]. Probability of failure was derived for combinations of the multivariate predictors using an exponential logistic equation with the fitted regression coefficients based on MLE [5]. The SPSS statistical package was utilized for regression analysis (version 12.0, SPSS Inc., Chicago, IL). Two-tailed values of $P<0.05$ were considered statistically significant.

Results

Descriptive statistics of densitometric, mechanical and morphometric properties are given in Tables 1 and 2 respectively. Apparent density ranged from 0.18 to 0.63 g/cm^3, yield strength from 0.32 to 2.25 MPa and the modulus of elasticity from 27 to 121 MPa for the specimens in this study. Average bone volume fraction for the 25 specimens ranged from 4.2% to 12.3%, whereas the volume fraction range for the weakest subregion ranged from 3.1% to 7.4% only. A power law model with BV/TV as the independent parameter described only 38% of the variation in the yield strength; however, the predictive power was increased to 56% when the BV/TV of the weakest subregion for each specimen was considered as the independent parameter.

The percentage of the weakest subregions overlapping the visually determined failure region was calculated for each index. In the 25 specimens analyzed in this study, 19 (76%) had minimum BV/TV and Conn.D values within the visually determined failure regions (Fig. 3). This percentage increased to 80% for BS/TV and for the fabric tensor in the principal direction of the trabecular network (H_1). The combination of BV/TV and H_1 increased the number of accurately predicted weakest links within the failure region to 88% (22 out of 25). The mean rank for each index was greater in the FX regions than in the NF regions. Further observations revealed that a cutoff rank value of 7.7 (out of 10) resulted in prediction of failure in the FX regions exclusively (no false positives from the NF regions). Additionally, the mean FX rank for each index for all 25 specimens was greater than the mean NF rank for each index.

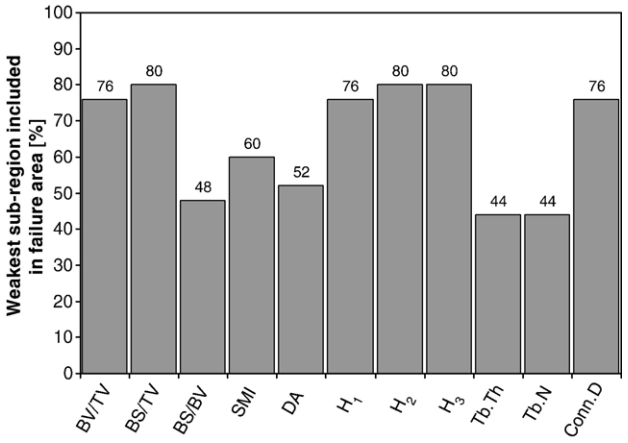

Fig. 3. Percentage of the weakest subregion (for each parameter) falling within the visually determined failure region.

A theoretical curve based on logistic regression analysis illustrates the probability of failure (as opposed to non-failure) based on BV/TV in Fig. 4. There was a significant inverse relationship between increasing values of BV/TV and the probability of failure as indicated by the likelihood ratio test ($P<0.001$). The probability curve is superimposed on the empirical numbers of FX and NF regions for specific intervals of BV/TV. For example, for BV/TV values less than 6%, there were a total of 42 regions demonstrating failure and 16 demonstrating non-failure. The abscissa represents intervals of BV/TV, and the left ordinate corresponds to the actual numbers of regions in each group (failure and non-failure). The right ordinate denotes the predicted probability of failure according to BV/TV.

Statistical analysis yielded significant differences in 8 morphometric indices between FX and NF regions. These indices included: BV/TV, BS/TV, Conn.D (all $P<0.01$) and SMI, Tb.Sp, H_1, H_2 and H_3 (all $P<0.05$). Multivariate logistic regression with the candidate variables consisting of the 8 significant parameters from univariate analysis resulted in a final model including 3 independent predictors. These parameters included: BV/TV, H_1 and Conn.D (likelihood ratio test (LRT)=11.69, 12.91 and 21.31 respectively, all $P<0.001$). Coefficients from the logistic regression equation were used to

Table 2
Descriptive statistics for morphometric analysis performed on all specimens

	BV/TV [%]	BS/TV [mm^2/mm^3]	BS/BV [mm^2/mm^3]	SMI	DA	H_1	H_2	H_3	Tb.Th [mm]	Tb.N [mm^{-1}]	Conn.D [mm^{-3}]
Mean	5.605	1.065	21.174	2.362	1.665	2.640	1.956	1.682	0.146	1.527	0.767
SD	1.183	0.220	2.052	0.165	0.150	0.591	0.434	0.360	0.010	0.053	0.380
Minimum	3.135	0.646	17.284	2.110	1.365	1.586	1.206	1.096	0.127	1.414	0.283
Maximum	7.437	1.641	24.636	2.666	1.940	4.050	2.994	2.721	0.176	1.633	1.834
CV (%)	21.11	20.65	9.69	6.99	8.98	22.40	22.17	21.40	7.03	3.48	49.52

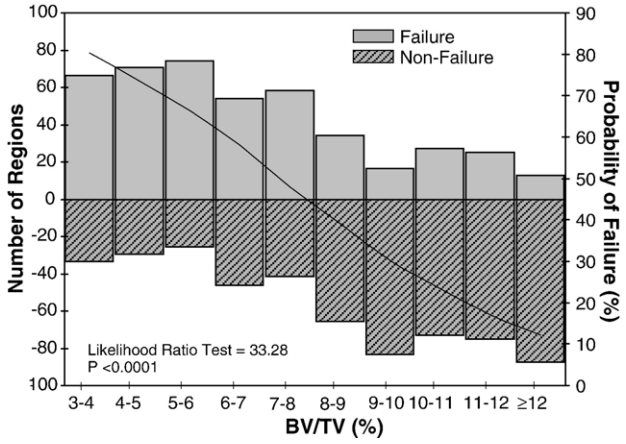

Fig. 4. A theoretical curve based on logistic regression analysis, illustrating the probability of failure (as opposed to non-failure) based on BV/TV values. Left end point convention was used for the BV/TV bins (for instance, the 5–6 bin ranges actually from 5 to 5.99).

derive a failure probability model (FPM) using the 3 independent variables.

$$\mathrm{FPM} = \frac{e^{(2-1.2\cdot\mathrm{Conn.D}-0.40\cdot\mathrm{BV/TV}+\mathrm{H_1})}}{1-e^{(2-1.2\cdot\mathrm{Conn.D}-0.40\cdot\mathrm{BV/TV}+\mathrm{H_1})}} \quad (1)$$

Varying the BV/TV values from 5 to 15%, the Conn.D from 1 to 4 mm^{-3} and H_1 from 1 to 4, four graphs are generated to predict fracture as illustrated in Figs. 5a–d. As the range of Conn.D is increased from 1 to 4, the probability of failure is decreased dramatically for all H_1 and BV/TV values. For instance, probability of failure is less than 14% for the worst-case scenario (lowest BV/TV and H_1 values) in Fig. 5d where Conn.D has a value of 4 mm^{-3}. This also holds true in Fig. 5c, with the exception of the lowest H_1 value, where the worst-case probability of failure is at 14% for Conn.D value of 3 mm^{-3}. Studying Fig. 5a in more detail reveals that, for a constant Conn.D value of 1 mm^{-3}, and BV/TV value of 10%, the probability of failure drops from 85% to 45% to 10% and finally to 2% respectively for H_1 values of 1, 2, 3 and 4.

The visualization of bone specimens in this study showed that failure mainly occurred in well-defined regions. Trabecular failure modes of buckling, barreling and rotation were observed, while locally, failure modes such as bending and buckling of individual trabecular elements were observed. The former were mostly seen in well-defined bands of horizontal or shear failure. Qualitative analysis of a number of specimens revealed that, in specimens with small variations in the BV/TV and trabecular microstructure, trabecular failure was initiated and remained in well-defined bands. The trabecular failure pattern could be described as the failure region folding over itself, much like of a building implosion, with most trabeculae failing in a bending mode. In specimens with larger microstructural variation (in the vertical direction), a trabecular failure pattern in the shear plane was observed. A general trend of bending and buckling was observed in plate-like structures, meanwhile rod-like trabeculae failed principally in buckling mode. In specimens where long plate-like structures were predominant throughout the structure, especially in the periphery, a pattern of barreling was observed where the plate-like elements started to bend around hinging points and eventually failed in barreling mode.

Discussion

The specimens in this study represented the lower segment of the volume fraction range for human cancellous bone. These findings were consistent with the values reported by Hildebrand et al., who showed the lumbar spine to be the site with the lowest average BV/TV values compared to other anatomic sites [10]. The range of BV/TV values was also reflected in the lower range of yield strength and modulus of elasticity for these specimens. The volume fraction range for the weakest subregions was noticeably smaller than the BV/TV range for the average specimens, suggesting that trabecular failure of the chain would occur at its weakest link. This notion is further strengthened by the significant increase in the predictive power of yield strength when BV/TV of the weakest subregion is used instead of the average specimen BV/TV. The low predictive power of yield strength in these specimens, in comparison to previously reported data [4,27], might be partially explained by the low range of specimen BV/TV, causing deviation from continuum mechanics principles. Analysis volume of these bones is not the same as normal bone since trabecular bone specimens with lower bone density tend to be more heterogeneous than those with density in the normal range. Additionally, the sizes of host bones where trabecular specimens can be cored from are finite. Therefore, specimen size variation is an inherent limitation of such studies as specimen size in a study cannot be changed easily due to constraints of host bone size and the adverse effects of varying specimen size on the study results. Further investigation is required to identify the cause(s) of this deviation.

Bone volume fraction plays an important role in assessing the structural integrity of trabecular bone, especially for bones with thinner than normal elements, where the trabecular microstructure is already compromised. The weakest region within the trabecular microstructure where failure actually occurs holds the key to the failure behavior of the entire specimen. The importance of BV/TV in predicting failure of subregions was investigated by logistic regression analysis. The approach iteratively tests values of BV/TV from failure and non-failure regions and converges a best fitting predictive curve for failure of cancellous bone specimens according to BV/TV values from specific regions within the specimen. In this model (Fig. 4), the inverse relationship between the increasing value of BV/TV and the probability of failure was demonstrated and showed good model fit. For example, the probability that a region with a BV/TV between 5 and 6% failed was 67%, whereas the probability of failure dropped to 13% for a BV/TV of 12% and higher.

A simple mean ranking model was used to rank subregions from most to least likely to fail (based on the sum of individual ranking for each trabecular index), and a subsequent experimental cutoff value appears to distinguish well between the FX and NF regions. This approach could be further investigated as an alternative method to predict failure in trabecular bone

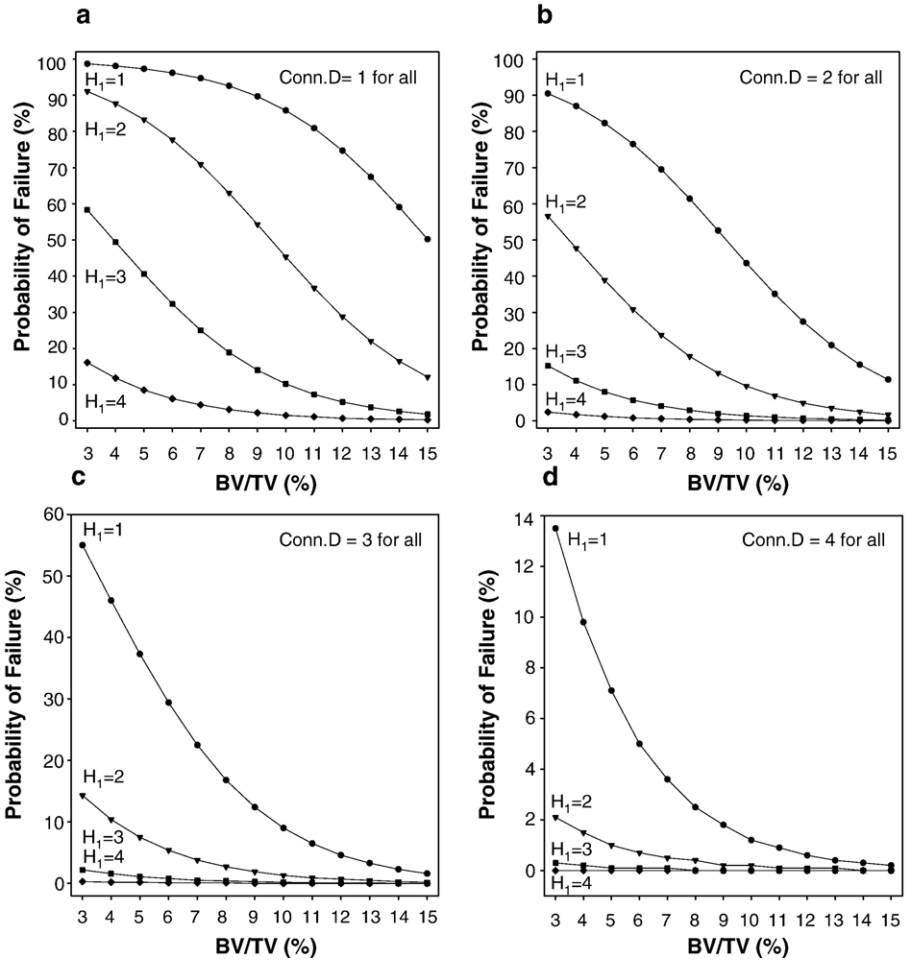

Fig. 5. Failure probability model [FPM] using 3 independent variables of BV/TV, H_1 and Conn.D. Conn.D value was varied from 1 to 4 mm^{-3} in figures a through d. The range of BV/TV and H1 values for each graph was from 3% to 15% and 1 to 4 respectively.

specimens. A simple comparison revealed that, in the majority of the cases (76%–88%), a combination of the lowest BV/TV, BS/TV, Conn.D or H_1 values closely correlated with the weakest subregion determined by visual inspection of failure. This finding highlights the importance of these structural parameters used in the context of identifying the weakest link in the chain. It is noteworthy that the exact region of failure could be predicted in 22 of 25 cases (88%) by a combination of BV/TV and H_1, which is a measure of spacing in the direction of highest anisotropy.

Statistical analysis of morphometric indices obtained in this study suggested that 8 indices yielded significant differences between the FX and NF regions. However, further multivariate logistic regression revealed that only three indices yielded independent significant differences between the FX and NF regions. These indices, BV/TV, Conn.D and H_1, were used to derive a probability failure model to help better predict failure in specimens in the lower BV/TV spectrum, an area where traditional average specimen parameters do not yield high predictive powers. This model illustrates the importance of these indices in the determination of strength of cancellous bone (Figs. 5a–d). Specifically, the contributions of Conn.D and H_1 are illustrated by the sharp declines in the failure probability as the range of Conn.D and H_1 values are increased. A limitation of any modeling approach is that equally sized specimens with similar inhomogeneity and same number of subregions are to be used in any subsequent attempt to use this model or any other model derived from these data.

This study shows that trabecular failure is locally initiated and can be predicted by morphometric indices. In many specimens, we observed large areas undergoing minimal deformation, whereas failure occurred in a visually discernable, well-defined band. The predominant mode of failure for the individual trabeculae includes bending and buckling, whereas compressive, shear and barreling failure modes were observed at the specimen level. Bending was visually observed to be the failure mode of choice for the plate-like structures, where bending would normally hinge upon a weak structural point along the length of the plate (such as a thinner area of the plate and a section of the plate where it was perforated). The rod-like structures predominantly failed in a buckling mode following Euler's criteria.

There is roughly a three-fold variation in the average bone volume fraction of specimens in this study, and all specimens were harvested from thoracic and lumbar regions of 2 donors with similar ages. In order to properly investigate the mechanical

behavior of cancellous bone under load, it will be important to carry out this type of study using whole bones as the behavior of cancellous bone at any site and within site is affected by its surrounding trabecular structure and the enveloping cortical shell. Technical limitations at the time of the study prevented us from undertaking such a study. Additionally, we were interested in evaluating the behavior of trabecular microstructure under load as a cellular solid outside the context of the whole bone.

Typical densitometry measurements do not take into account local variations of the trabecular microstructure or the non-uniform distribution of trabecular elements and failure regions. As a result, standard densitometry can only generate accurate results if bone microstructure is distributed uniformly, an important criterion not met for most pathological cases. To this end, we have shown that, alternatively, the subregions with the lowest bone volume fraction values are better suited to predict mechanical failure in cancellous bone specimens. This predictive power is augmented even more by taking into consideration additional microstructural indices in an effort to generate a failure prediction model based on bone volume fraction and microstructural distribution of cancellous bone specimens specifically in areas where failure is most likely to occur.

Acknowledgments

This study was partially funded by a Biomedical Engineering Research Grant of the Whitaker Foundation and the SNF Professorship in Bioengineering of the Swiss National Science Foundation (FP 620-58097.99). The authors would like to acknowledge the staff at the Orthopedic Biomechanics Laboratory at Beth Israel Deaconess Medical Center, especially Fraser Harrold for his help with specimen collection, and the Bioelectronics Group at the Swiss Federal Institute of Technology for their support.

References

[1] Diagnostic and therapeutic technology assessment. Measurement of bone density with dual-energy X-ray absorptiometry (DEXA). JAMA 1992; 267: 286–8, 290–4.
[2] Osteoporosis prevention, diagnosis, and therapy. NIH Consens Statement 2000;17:1–45.
[3] Beck T. Measuring the structural strength of bones with dual-energy X-ray absorptiometry: principles, technical limitations, and future possibilities. Osteoporos Int 2003;14(Suppl 14):81–8.
[4] Carter DR, Hayes WC. Bone compressive strength: the influence of density and strain rate. Science 1976;194:1174–6.
[5] Cox DR. Analysis of Binary Data. 2nd ed. New York: Chapman and Hall; 1989. p. 33–49.
[6] Gibson LJ. Biomechanics of cellular solids. J Biomech 2005;38: 377–99.
[7] Gomberg BR, Saha PK, Wehrli FW. Topology-based orientation analysis of trabecular bone networks. Med Phys 2003;30:58–68.
[8] Hahn M, Vogel M, Pompesius-Kempa M, Delling G. Trabecular bone pattern factor—A new parameter for simple quantification of bone microarchitecture. Bone 1992;13:327–30.
[9] Harrigan TP, Mann RW. Characterization of microstructural anisotropy in orthotropic materials using a second rank tensor. J Mater Sci 1984;19:761–7.
[10] Hildebrand T, Laib A, Muller R, Dequeker J, Ruegsegger P. Direct three-dimensional morphometric analysis of human cancellous bone: microstructural data from spine, femur, iliac crest, and calcaneus. J Bone Miner Res 1999;14:1167–74.
[11] Hosmer DW, Lemeshow S. Applied Logistic Regression. 2nd ed. New York: John Wiley; 2000. p. 47–69.
[12] Hosmer DW, Hosmer T, Le Cessie S, Lemeshow S. A comparison of goodness-of-fit tests for the logistic regression model. Stat Med 1997;16:965–80.
[13] Keaveny TM, Borchers RE, Gibson LJ, Hayes WC. Theoretical analysis of the experimental artifact in trabecular bone compressive modulus. J Biomech 1993;26:599–607.
[14] Keaveny TM, Borchers RE, Gibson LJ, Hayes WC. Trabecular bone modulus and strength can depend on specimen geometry. J Biomech 1993;26:991–1000.
[15] Keaveny TM, Pinilla TP, Crawford RP, Kopperdahl DL, Lou A. Systematic and random errors in compression testing of trabecular bone. J Orthop Res 1997;15:101–10.
[16] Lorensen WE, Cline HE. Marching cubes: a high resolution 3D surface construction algorithm. Comput Graph 1987;21:163–9.
[17] Mosekilde L. Age-related changes in vertebral trabecular bone architecture-assessed by a new method. Bone 1988;9:247–50.
[18] Muller R, Gerber SC, Hayes WC. Micro-compression: a novel technique for the nondestructive assessment of local bone failure. Technol Health Care 1998;6:433–44.
[19] Muller R, Hannan M, Smith SY, Bauss F. Intermittent ibandronate preserves bone quality and bone strength in the lumbar spine after 16 months of treatment in the ovariectomized cynomolgus monkey. J Bone Miner Res 2004;19:1787–96.
[20] Muller R, Hildebrand T, Ruegsegger P. Non-invasive bone biopsy: a new method to analyse and display the three-dimensional structure of trabecular bone. Phys Med Biol 1994;39:145–64.
[21] Muller R, Ruegsegger P. Micro-tomographic imaging for the nondestructive evaluation of trabecular bone architecture. Stud Health Technol Inform 1997;40:61–79.
[22] Nazarian A, Muller R. Time-lapsed microstructural imaging of bone failure behavior. J Biomech 2004;37:55–65.
[23] Nazarian A, Stauber M, Muller R. Design and implementation of a novel mechanical testing system for cellular solids. J Biomed Mater Res, B Appl Biomater 2005;73:400–11.
[24] Odgaard A. Three-dimensional methods for quantification of cancellous bone architecture. Bone 1997;20:315–28.
[25] Odgaard A, Gundersen HJ. Quantification of connectivity in cancellous bone, with special emphasis on 3-D reconstructions. Bone 1993;14: 173–182.
[26] Parfitt AM. Trabecular bone architecture in the pathogenesis and prevention of fracture. Am J Med 1987;82:68–72.
[27] Rice JC, Cowin SC, Bowman JA. On the dependence of the elasticity and strength of cancellous bone on apparent density. J Biomech 1988;21: 155–68.
[28] Ruegsegger P, Koller B, Muller R. A microtomographic system for the nondestructive evaluation of bone architecture. Calcif Tissue Int 1996;58:24–9.
[29] Silva MJ, Gibson LJ. Modeling the mechanical behavior of vertebral trabecular bone: effects of age-related changes in microstructure. Bone 1997;21:191–9.